The Astrophysical Journal, 927:47 (5pp), 2022 March 1 https://doi.org/10.3847/1538-4357/ac41ce

Branching Ratio for $O + H_3^+$ Forming $OH^+ + H_2$ and $H_2O^+ + H$

Pierre-Michel Hillenbrand[1,2], Nathalie de Ruette[1,3], Xavier Urbain[4], and Daniel W. Savin[1]
[1] Columbia Astrophysics Laboratory, Columbia University, New York, NY 10027, U.S.A.
[2] Institut für Kernphysik, Goethe-Universität, D-60438 Frankfurt, Germany
[3] European Spallation Source ERIC, SE-22100 Lund, Sweden
[4] Institute of Condensed Matter and Nanosciences, Université catholique de Louvain, B-1348 Louvain-la-Neuve, Belgium
Received 2021 October 27; revised 2021 December 2; accepted 2021 December 8; published 2022 March 3

Abstract

The gas-phase reaction of $O + H_3^+$ has two exothermic product channels: $OH^+ + H_2$ and $H_2O^+ + H$. In the present study, we analyze experimental data from a merged-beams measurement to derive thermal rate coefficients resolved by product channel for the temperature range from 10 to 1000 K. Published astrochemical models either ignore the second product channel or apply a temperature-independent branching ratio of 70% versus 30% for the formation of $OH^+ + H_2$ versus $H_2O^+ + H$, respectively, which originates from a single experimental data point measured at 295 K. Our results are consistent with this data point, but show a branching ratio that varies with temperature reaching 58% versus 42% at 10 K. We provide recommended rate coefficients for the two product channels for two cases, one where the initial fine-structure population of the $O(^3P_J)$ reactant is in its $J = 2$ ground state and the other one where it is in thermal equilibrium.

Unified Astronomy Thesaurus concepts: Interstellar molecules (849); Molecular clouds (1072); Collision processes (2065); Molecule destruction (2075); Molecule formation (2076)

1. Introduction

At the low temperatures typical of diffuse and dense molecular clouds (~10–100 K), gas-phase formation of water is dominated by a sequence of exothermic ion-neutral reactions (van Dishoeck et al. 2013). Two parallel formation pathways have been identified: One pathway proceeds via the reaction

$$O + H_3^+ \rightarrow \begin{cases} OH^+ + H_2 + 0.66\,\text{eV} & \text{(1a)} \\ H_2O^+ + H + 1.70\,\text{eV}, & \text{(1b)} \end{cases}$$

which is the focus of the present paper. The quoted energies represent the exoergicities of the reactions provided by Milligan & McEwan (2000). The other pathway proceeds via cosmic-ray ionization of O to O^+ or endothermic charge transfer with H^+, produced by cosmic-ray ionization of H and H_2, and the subsequent reaction (Bulut et al. 2015; Kovalenko et al. 2018):

$$O^+ + H_2 \rightarrow OH^+ + H. \quad (2)$$

Both pathways are followed by the reactions (Tran et al. 2018; Kumar et al. 2018):

$$OH^+ \xrightarrow{H_2} H_2O^+ \xrightarrow{H_2} H_3O^+. \quad (3)$$

Dissociative recombination (DR) of electrons with H_3O^+ then leads to the formation of H_2O (Novotný et al. 2010). Two other important ingredients for an accurate gas-phase reaction network for forming water are the DR rate coefficients leading to the destruction of OH^+ (Amitay et al. 1996; Stroe & Fifirig 2018) and H_2O^+ (Rosén et al. 2000; Nkambule et al. 2015).

The various routes of interstellar water chemistry, including reactions (1)–(3), have been reviewed by van Dishoeck et al. (2013, 2021). The branching ratio for reaction (1b) is particularly important for describing the ortho-to-para ratio of water in interstellar clouds (Faure et al. 2019). Furthermore, the observed abundances of OH^+, H_2O^+, and H_3O^+ are used to infer the cosmic-ray ionization rate (Hollenbach et al. 2012; Indriolo et al. 2015; Neufeld & Wolfire 2017; Indriolo et al. 2018). At temperatures of ~250 K, endothermic neutral–neutral reactions such as $O + H_2 \rightarrow OH + H$ become accessible and dominate the gas-phase water formation process (van Dishoeck et al. 2021). This sets an upper limit for the temperature range of interest for reactions (1)–(3).

In the present paper, we investigate the temperature-dependent thermal rate coefficients and branching ratios for reactions (1a) and (1b). We derive our results from the merged-beams experiment performed by de Ruette et al. (2016). In their work, they derived the thermal rate coefficient for the sum over both product channels, but not those resolved by product channel. We provide the relevant details of the experimental data set in Section 2. In Section 3, we present our results and compare them to the data available in the literature. Finally, in Section 4, we discuss possible implications of our results on astrochemical models.

2. Experimental Data

In the merged-beams experiment of de Ruette et al. (2016), a beam of atomic oxygen was overlapped with a beam of H_3^+ at a well-defined relative collision energy. The product ions, either OH^+ or H_2O^+, were counted, normalized to the intensities of the two parent beams and the interaction volume, and corrected for transmittance and detection efficiencies. The particle densities in the interaction volume were low enough to exclude the formation of H_2O^+ by sequential collisions.

From the data, absolute cross sections as a function of the relative collision energy, E_r, were derived for each product channel individually. The range of E_r was 3.5 meV to 15.5 eV

Table 1
Parameters for $\sigma_x(E_r)$ Defined in Equation (4)

Parameter	Product Channel x	
	$OH^+ + H_2$[a]	$H_2O^+ + H$
a_0	1.1880×10^{-16}	9.8531×10^{-17}
$a_{1/2}$	5.1976×10^{-16}	...
b_1	...	-4.0668×10^{-2}
b_2	7.3434×10^{-2}	-4.1891
b_4	8.3488×10^{-4}	5.1780×10^{2}

Note.
[a] The values for this reaction were misprinted in de Ruette et al. (2016).

and 3.5 meV to 130 meV for the OH^+ and H_2O^+ products, respectively. At values of E_r higher than the ones investigated, the individual cross sections were smaller than the detection sensitivity of the experiment.

The data for each product channel was parameterized by the fit function:

$$\sigma_x(E_r) = \frac{a_0 + a_{1/2}E_r^{1/2}}{E_r^{2/3} + b_1E_r + b_2E_r^2 + b_4E_r^4}. \quad (4)$$

Here, $x = \{OH^+, H_2O^+\}$ refers to reactions (1a) and (1b), respectively, σ_x is in units of cm^2, and E_r is in eV. The $\sim E_r^{-2/3}$ scaling in the limit of $E_r \to 0$ reflects the effect of the long-range charge–quadrupole interaction between the H_3^+ ion and the oxygen atom, as was discussed by Klippenstein et al. (2010). The fit parameters are given in Table 1. The total uncertainty of the cross sections was given by the fitting uncertainty and the relative systematic uncertainty of 13%, both summed in quadrature.

Considering the astrochemical motivation of this study and the range of measured collision energies, we derived translational rate coefficients, $k_x^{tr}(T)$, in the temperature range of $T = 10$–1000 K by convoluting each cross section times the relative collision velocity, $\sigma_x(E_r) \times v_r$, with a Maxwell–Boltzmann distribution. The uncertainties of the rate coefficients were propagated from the total uncertainties of the cross sections. Furthermore, we define the branching ratios, $f_x(T)$, as the relative yields:

$$f_{OH^+} = \frac{k^{tr}_{OH^+}}{k^{tr}_{OH^+} + k^{tr}_{H_2O^+}}, \quad (5a)$$

$$f_{H_2O^+} = \frac{k^{tr}_{H_2O^+}}{k^{tr}_{OH^+} + k^{tr}_{H_2O^+}}. \quad (5b)$$

The uncertainty of $f_x(T)$ is solely affected by statistical fluctuations, while the systematic uncertainty cancels out. In the considered temperature range, the relative uncertainties of f_{OH^+} and $f_{H_2O^+}$ range from 3% to 5% and 5% to 12%, respectively, while the absolute magnitude of the uncertainty is identical for both branching ratios.

To understand the relation between $k_x^{tr}(T)$ and the thermal rate coefficient, $k_x(T)$, we will discuss the role of the internal excitation of the two reactants in Sections 2.1 and 2.2, respectively.

2.1. The H_3^+ Reactant

The merged-beams experiment of de Ruette et al. (2016) was performed with an internally excited H_3^+ beam. Most of the possible influences of this internal excitation on the measured merged-beams rate coefficient were discussed in their publication. In the experiment, the internal temperature of the H_3^+ ions was estimated to be $T_{int} \approx 2500$–3000 K. In Hillenbrand et al. (2019), we performed a more detailed analysis of the H_3^+ internal temperature and its dependency on the H_2 pressure in the ion source. From those results, we confirmed that the H_2 pressure applied in the measurements of de Ruette et al. (2016) corresponds consistently to the previously estimated internal temperature. Here, we discuss an additional aspect of the H_3^+ internal temperature that was not considered in de Ruette et al. (2016).

For comparison, the exothermic reaction of $C + H_2^+ \to CH^+ + H$ was studied in Hillenbrand et al. (2020). In that reaction, a low-lying endoergic reaction channel forming $C^+ + H + H$ is energetically accessible at zero translational energy, provided that the internal excitation of the H_2^+ reactant is sufficiently high. We found that this considerably reduced the measured merged-beams rate coefficient for all translational energies investigated.

For the reaction studied here, the lowest endoergic channel is (de Ruette et al. 2016)

$$O + H_3^+ \to OH + H_2^+ - 1.77\ \text{eV}. \quad (6)$$

We can estimate the fraction of H_3^+ ions, whose internal energy is above this threshold, $E_{int} > E_{th} = 1.77$ eV, for a given internal temperature of T_{int} by integrating the Boltzmann distribution over the internal energy,

$$f_{E_{int}>E_{th}} = 1 - \frac{1}{\langle E_{int}\rangle}\int_0^{E_{th}} \exp\left(-\frac{E_{int}}{\langle E_{int}\rangle}\right) dE_{int} = \exp\left(-\frac{E_{th}}{\langle E_{int}\rangle}\right). \quad (7)$$

Based on the partition function provided by Kylänpää & Rantala (2011), $T_{int} = 2500$ and 3000 K correspond to mean internal energies of $\langle E_{int}\rangle = 0.64$ and 0.86 eV, where 6%–13% of the H_3^+ ions have an internal energy above E_{th}, respectively. A part of this fraction can potentially form $OH + H_2^+$, even at the lowest measured translational energies. As a worst-case scenario, we can assume that all reactions of H_3^+ ions with $E_{int} > E_{th}$ do not contribute to reactions (1a) or (1b). This would mean that the cross sections and rate coefficients reported by de Ruette et al. (2016) need to be scaled up by a factor 1.06–1.15. This scaling lies well within the total experimental uncertainty limits. Moreover, it affects both channels in the same direction and therefore does not affect the branching ratios.

2.2. The $O(^3P_J)$ Reactant

In de Ruette et al. (2016), the atomic oxygen beam was generated through laser photodetachment of an oxygen anion beam (O'Connor et al. 2015b). The resulting oxygen atoms were in the ^3P_J ground term and the fine structure levels were populated according to their multiplicity, with fractional populations being $5/9$, $3/9$, and $1/9$ for $J = 2$, 1, and 0,

respectively. This statistical population was verified at the few percent level in the experiment of Génévriez et al. (2018).

For $O(^3P_J)$, $J=2$ represents the ground level, while the $J=1$ and the $J=0$ levels are excited by $E_1=19.6$ meV and $E_0=28.1$ meV, respectively (Lique et al. 2018). The three fine-structure levels comprise a total of nine magnetic sublevels. As first pointed out by Gentry & Giese (1977), only the three sublevels corresponding to $J=2$ with $M_J=\pm1$ or $M_J=0$ correlate to the reactive $^3\Sigma$ potential energy surface (PES). The other six sublevels all correlate with the nonreactive $^3\Pi$ PES (Gentry & Giese 1977; Bettens et al. 1999; Klippenstein et al. 2010). Since both product channels only proceed on the $^3\Sigma$ PES, the branching ratio of the product channels is independent of the initial fine-structure population. This aspect was overlooked by de Ruette et al. (2016) and prevented them from deriving thermal rate coefficients for the individual product channels.

Two astrochemical scenarios for the fine-structure level population may be of interest: Either only the $J=2$ ground level is populated or the fine-structure level populations are in thermal equilibrium. Which of the two cases is applicable actually depends on the particle density. According to Lique et al. (2018), atomic oxygen is thermalized only at H or H_2 densities on the order of 10^6–10^7 cm^{-3}.

The conversion of the measured translational rate coefficients into thermal rate coefficients assuming a statistical population of the fine-structure levels in the merged-beams experiment and a thermal population in the astrochemical environment is (de Ruette et al. 2016)

$$k_x(T) = k_x^{\mathrm{tr}}(T) \times \frac{9}{5 + 3\exp(-E_1/k_\mathrm{B}T) + \exp(-E_0/k_\mathrm{B}T)}. \quad (8)$$

Here, k_B is the Boltzmann constant. For the scenario of a pure $O(^3P_2)$ reactant, the relation reduces to $k_x(T) = k_x^{\mathrm{tr}}(T) \times 9/5$. As discussed above, the rate coefficients for $O(^3P_1)$ and $O(^3P_0)$ reactants are zero for both scenarios.

3. Thermal Rate Coefficient

3.1. Summed over Both Product Channels

The thermal rate coefficient summed over both product channels, assuming a thermal population of the $O(^3P_J)$ fine-structure levels, has been discussed in detail by de Ruette et al. (2016). The temperature dependency of the thermal rate coefficient is mainly formed by the effect of the long-range charge–quadrupole interaction [see Equation (4)], and the effect of the fine-structure population [see Equation (8)]. The results were compared to two published experimental data points, both measured at room temperature: Fehsenfeld (1976) used a flowing afterglow technique to measure the thermal rate coefficient summed over both product channels, and Milligan & McEwan (2000) applied a combined flowing afterglow/selected ion flow tube technique to measure thermal rate coefficients resolved by product channel. Both methods are such that the translational temperature and the internal temperature of both reactants were in thermal equilibrium. The results of de Ruette et al. (2016) were in good agreement with the measurement of Fehsenfeld (1976) and in reasonable agreement with the measurements of Milligan & McEwan (2000). Furthermore, the theoretical rate coefficients of Bettens et al. (1999) and Klippenstein et al. (2010) had the same temperature dependency as the result of de Ruette et al. (2016), but were overall a factor of about 1.5 higher. Following the discussion of Section 2.1 it is unlikely that such a discrepancy was caused by the internal excitation of the H_3^+ beam in the experiment.

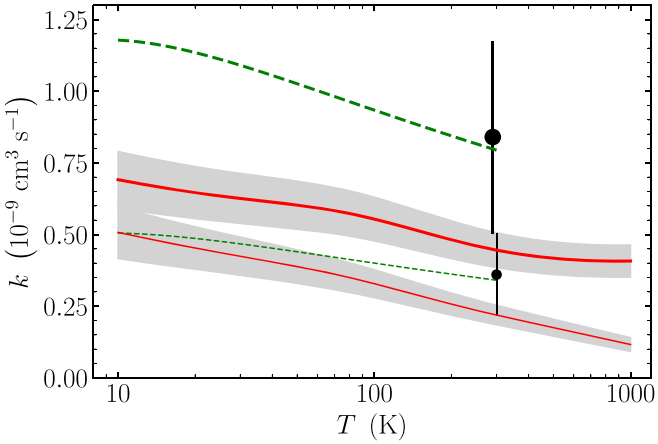

Figure 1. Thermal rate coefficient for the $OH^+ + H_2$ channel (upper bold data) and the $H_2O^+ + H$ channel (lower fine data). Shown are: our results by the red solid lines, with the gray area indicating the total experimental uncertainty at one standard deviation; the results of Milligan & McEwan (2000) by the circular data points (shifted slightly in temperature for clarity); and the data implemented in the astrochemical models listed in Section 3.2 by the green dashed lines.

3.2. Resolved by Product Channel

The thermal rate coefficients resolved by product channel, derived from the data of de Ruette et al. (2016), are shown in Figure 1. Considering the mutual uncertainties, they agree reasonably well with the measurement of Milligan & McEwan (2000) at 295 K. Astrochemical models such as UMIST (McElroy et al. 2013), KIDA (Wakelam et al. 2015), and UGAN (Hily-Blant et al. 2018) implemented channel resolved rate coefficients using the total reaction rate coefficient of Klippenstein et al. (2010) and the branching ratio from Milligan & McEwan (2000), and assumed the ratio to be temperature-independent. Our results are generally lower than the rates implemented in the models. Of particular note is the factor 1.7 difference at 10 K for the $OH^+ + H_2$ channel.

3.3. Branching Ratio

The branching ratio defined in Equation (5) is plotted in Figure 2. For the $H_2O^+ + H$ product channel, the branching ratio derived from our results ranges from (42 ± 3)% at 10 K down to (22 ± 3)% at 1000 K. At 295 K, our result of (33 ± 2)% is consistent with the value of (30 ± 9)% measured by Milligan & McEwan (2000). Up to now, those astrochemical models that considered the branching ratio assumed it to be 30% independent of the temperature, based on the measurement of Milligan & McEwan (2000).

The branching ratio calculated by Bettens et al. (1999) was (5.6 ± 1.6)% for the $H_2O^+ + H$ product channel, and thus does not agree at all with either set of experimental results. For the analog reaction of $C + H_3^+$, we found a similar discrepancy between our experimental results in O'Connor et al. (2015a) and the theoretical results of Bettens & Collins (1998, 2001). These findings may suggest a shortcoming of the classical

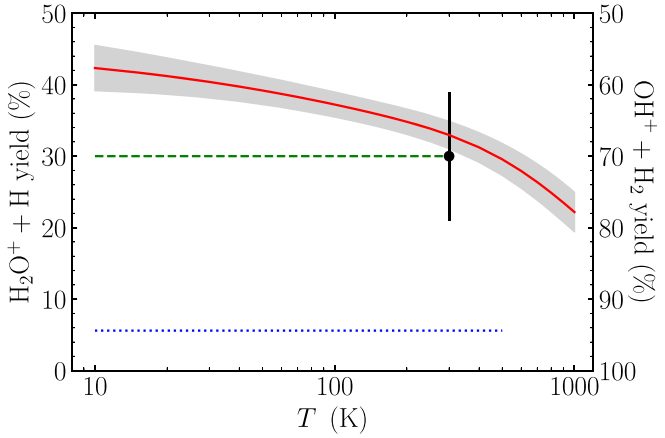

Figure 2. Branching ratio expressed as relative yield for the two product channels. Shown are: our results by the red solid line, with the gray area indicating the total experimental uncertainty at one standard deviation; the results of Milligan & McEwan (2000) by the circular data point; the results of Bettens et al. (1999) by the blue dotted line; and the ratio implemented in the astrochemical models listed in Section 3.2 by the green dashed line.

trajectory simulations and the PES used. The good agreement for the branching ratio for $O + H_3^+$ from the experimental results of Milligan & McEwan (2000) and our results in de Ruette et al. (2016), which used two different experimental methods with differing systematics, and for $C + H_3^+$ from Savić et al. (2005) and ours in O'Connor et al. (2015a), which also used two different experimental methods with differing systematics, suggest that the discrepancy is not an experimental issue.

3.4. Recommended Rate Coefficients

We used the Arrhenius–Kooij formula,

$$k(T) = \alpha\left(\frac{T}{300\ \mathrm{K}}\right)^{\beta}\exp\left(-\frac{\gamma}{T}\right), \tag{9}$$

to parameterize our results for the two product channels in the temperature range of 10–1000 K for implementation into astrochemical models. The fit parameters, α, β, and γ, are shown in Table 2 for the two cases of the $O(^3P_J)$ level population discussed in Section 2.2 and the two product channels. The fits describe our results to better than 5% for reaction (1a) and to better than 10% for reaction (1b).

Resolved by the nuclear-spin states, reactions (1a) and (1b) read

$$\mathrm{O} + \text{p-}\mathrm{H_3^+} \rightarrow \begin{cases} \mathrm{OH^+} + \text{p-}\mathrm{H_2} & [1/2] \quad (10a) \\ \mathrm{OH^+} + \text{o-}\mathrm{H_2} & [1/2] \quad (10b) \\ \text{p-}\mathrm{H_2O^+} + \mathrm{H} & [1/2] \quad (10c) \\ \text{o-}\mathrm{H_2O^+} + \mathrm{H} & [1/2] \quad (10d) \end{cases}$$

and

$$\mathrm{O} + \text{o-}\mathrm{H_3^+} \rightarrow \begin{cases} \mathrm{OH^+} + \text{o-}\mathrm{H_2} & [1] \quad (11a) \\ \text{o-}\mathrm{H_2O^+} + \mathrm{H} & [1], \quad (11b) \end{cases}$$

where p- signifies para and o- signifies ortho. In reactions (10) and (11), the numbers given in squared brackets represent the statistical factors resulting from the nuclear-spin selection rules (Oka 2004). In nuclear-spin state resolved astrochemical networks, the rate coefficients are typically scaled by multiplying the parameters α with the statistical factor while the parameters β and γ are considered to be independent of the spin states (Majumdar et al. 2017; Hily-Blant et al. 2018). This approach is justified for reactions where the exoergicity does not differ significantly between different spin-resolved product channels. The same approach can be applied to our results given in Table 2, and the resulting nuclear-spin-resolved rate coefficients can be implemented into models studying the ortho-to-para ratio of gas-phase-formed water (Faure et al. 2019).

Table 2
Recommended Thermal Rate Coefficients for $O + H_3^+$, Given as Parameters of Equation (9) for $T = 10$–1000 K

$O(^3P_J)$ Population	Product Channel	α (10^{-9} cm^3 s^{-1})	β	γ (K)
$J = 2$	$OH^+ + H_2$	0.612	0.05	−3.08
	$H_2O^+ + H$	0.271	−0.21	0.57
J thermal	$OH^+ + H_2$	0.465	−0.14	0.67
	$H_2O^+ + H$	0.208	−0.40	4.86

4. Astrochemical Implications

In de Ruette et al. (2016), the derived thermal rate coefficient summed over both product channels was implemented into the KIDA model (Wakelam et al. 2015), and potential implications were studied for the predicted abundances of H_3O^+, H_2O, and other molecules downstream the reaction chain. Here, we briefly discuss the relevance of the $O + H_3^+$ branching ratio along the following simplified reaction chain:

$$\mathrm{O} \xrightarrow{\mathrm{H_3^+}} \begin{cases} \mathrm{OH^+} + \mathrm{H_2} \begin{cases} \xrightarrow{\mathrm{H_2}} \mathrm{H_2O^+} + \mathrm{H} + \mathrm{H_2} \\ \xrightarrow{\mathrm{e^-}} \mathrm{O} + \mathrm{H} + \mathrm{H_2} \end{cases} \\ \mathrm{H_2O^+} + \mathrm{H}. \end{cases} \tag{12}$$

For typical astrochemical environments, the H_2 density is high enough such that the H_2O^+ formation through the intermediate step of OH^+ formation proceeds with an effective rate coefficient comparable to the direct formation pathway. In this case, including the branching ratio decreases the predicted OH^+ abundance, but not the H_2O^+ abundance nor subsequent products along the reaction chain, such as H_3O^+ and, prominently, H_2O. However, in those scenarios where the destruction of OH^+ by DR plays a significant role, direct formation of H_2O^+ presents a bypass with respect to the OH^+ destruction by DR, and thus may enhance the abundance of H_2O^+ and its subsequent reaction products.

5. Summary

Based on the experimental data of de Ruette et al. (2016), we have derived temperature-dependent thermal rate coefficients for reactions (1a) and (1b). The experimental data were measured with internally excited H_3^+ reactants, but we find that this has no significant effect on the derived rate coefficients.

Up to now, the general understanding for the branching ratio of these reactions relied solely on the fixed temperature measurement of Milligan & McEwan (2000) at 295 K. At that temperature, we found a branching ratio that is consistent with the one implemented in commonly used astrochemical models, but we find an enhanced yield for the $H_2O^+ + H$ product

channel toward lower temperatures. Our results underline the importance of including both product channels into reliable models.

This research was supported, in part, by the NSF Division of Astronomical Sciences Astronomy and Astrophysics Grants program under AST-2002461. X.U. is a Senior Research Associate of the Fonds de la Recherche Scientifique-FNRS.

ORCID iDs

Pierre-Michel Hillenbrand https://orcid.org/0000-0003-0166-2666
Nathalie de Ruette https://orcid.org/0000-0002-9950-4449
Xavier Urbain https://orcid.org/0000-0003-3326-8823
Daniel W. Savin https://orcid.org/0000-0002-1111-6610

References

Amitay, Z., Zajfman, D., Forck, P., et al. 1996, PhRvA, 53, R644
Bettens, R. P. A., & Collins, M. A. 1998, JChPh, 108, 2424
Bettens, R. P. A., & Collins, M. A. 2001, JChPh, 114, 6490
Bettens, R. P. A., Hansen, T. A., & Collins, M. A. 1999, JChPh, 111, 6322
Bulut, N., Castillo, J. F., Jambrina, P. G., et al. 2015, JPCA, 119, 11951
de Ruette, N., Miller, K. A., O'Connor, A. P., et al. 2016, ApJ, 816, 31
Faure, A., Hily-Blant, P., Rist, C., et al. 2019, MNRAS, 487, 3392
Fehsenfeld, F. C. 1976, ApJ, 209, 638
Génévriez, M., Dunseath, K. M., Terao-Dunseath, M., et al. 2018, PhRvA, 98, 033410
Gentry, W. R., & Giese, C. F. 1977, JChPh, 67, 2355
Hillenbrand, P.-M., Bowen, K. P., Dayou, F., et al. 2020, PCCP, 22, 27364
Hillenbrand, P.-M., Bowen, K. P., Liévin, J., Urbain, X., & Savin, D. W. 2019, ApJ, 877, 38
Hily-Blant, P., Faure, A., Rist, C., Pineau des Forêts, G., & Flower, D. R. 2018, MNRAS, 477, 4454
Hollenbach, D., Kaufman, M. J., Neufeld, D., Wolfire, M., & Goicoechea, J. R. 2012, ApJ, 754, 105
Indriolo, N., Bergin, E. A., Falgarone, E., et al. 2018, ApJ, 865, 127
Indriolo, N., Neufeld, D. A., Gerin, M., et al. 2015, ApJ, 800, 40
Klippenstein, S. J., Georgievskii, Y., & McCall, B. J. 2010, JPCA, 114, 278
Kovalenko, A., Tran, T. D., Rednyk, S., et al. 2018, ApJ, 856, 100
Kumar, S. S., Grussie, F., Suleimanov, Y. V., Guo, H., & Kreckel, H. 2018, SciAd, 4, eaar3417
Kylänpää, I., & Rantala, T. T. 2011, JChPh, 135, 104310
Lique, F., Kłos, J., Alexander, M. H., Le Picard, S. D., & Dagdigian, P. J. 2018, MNRAS, 474, 2313
Majumdar, L., Gratier, P., Ruaud, M., et al. 2017, MNRAS, 466, 4470
McElroy, D., Walsh, C., Markwick, A. J., et al. 2013, A&A, 550, A36
Milligan, D. B., & McEwan, M. J. 2000, CPL, 319, 482
Neufeld, D. A., & Wolfire, M. G. 2017, ApJ, 845, 163
Nkambule, S. M., Larson, Å., Fonseca dos Santos, S., & Orel, A. E. 2015, PhRvA, 92, 012708
Novotný, O., Buhr, H., Stützel, J., et al. 2010, JPCA, 114, 4870
O'Connor, A. P., Grussie, F., Bruhns, H., et al. 2015b, RScI, 86, 113306
O'Connor, A. P., Urbain, X., Stützel, J., et al. 2015a, ApJS, 219, 6
Oka, T. 2004, JMoSp, 228, 635
Rosén, S., Derkatch, A., Semaniak, J., et al. 2000, FaDi, 115, 295
Savić, I., Čermák, I., & Gerlich, D. 2005, IJMSp, 240, 139
Stroe, M. C., & Fifirig, M. 2018, JPhB, 51, 025202
Tran, T. D., Rednyk, S., Kovalenko, A., et al. 2018, ApJ, 854, 25
van Dishoeck, E. F., Herbst, E., & Neufeld, D. A. 2013, ChRv, 113, 9043
van Dishoeck, E. F., Kristensen, L. E., Mottram, J. C., et al. 2021, A&A, 648, A24
Wakelam, V., Loison, J.-C., Herbst, E., et al. 2015, ApJS, 217, 20